ARMY RESEARCH LABORATORY

Energy Partitioning and Impulse Dispersion in the Decorated, Tapered, Strongly Nonlinear Granular Alignment: A System With Many Potential Applications

by Robert L. Doney, Juan H. Agui, and Surajit Sen

NOTICES

Disclaimers

The findings in this report are not to be construed as an official Department of the Army position unless so designated by other authorized documents.

Citation of manufacturer's or trade names does not constitute an official endorsement or approval of the use thereof.

Destroy this report when it is no longer needed. Do not return it to the originator.

Army Research Laboratory

Aberdeen Proving Ground, MD 21005-5066

Energy Partitioning and Impulse Dispersion in the Decorated, Tapered, Strongly Nonlinear Granular Alignment: A System With Many Potential Applications

Robert L. Doney
Weapons and Materials Research Directorate, ARL

Juan H. Agui
NASA-Glenn Research Center

Surajit Sen
State University of New York

REPORT DOCUMENTATION PAGE

Form Approved OMB No. 0704-0188

1. REPORT DATE *(DD-MM-YYYY)*	2. REPORT TYPE	3. DATES COVERED (From - To)
March 2010	Reprint	August 2008–September 2009

4. TITLE AND SUBTITLE	5a. CONTRACT NUMBER
Energy Partitioning and Impulse Dispersion in the Decorated, Tapered, Strongly Nonlinear Granular Alignment: A System With Many Potential Applications	
	5b. GRANT NUMBER
	5c. PROGRAM ELEMENT NUMBER
6. AUTHOR(S)	5d. PROJECT NUMBER
Robert L. Doney, Juan H. Agui,[*] and Surajit Sen[†]	
	5e. TASK NUMBER
	5f. WORK UNIT NUMBER

7. PERFORMING ORGANIZATION NAME(S) AND ADDRESS(ES)	8. PERFORMING ORGANIZATION REPORT NUMBER
U.S. Army Research Laboratory ATTN: RDRL-WMT-A Aberdeen Proving Ground, MD 21005-5066	ARL-RP-289

9. SPONSORING/MONITORING AGENCY NAME(S) AND ADDRESS(ES)	10. SPONSOR/MONITOR'S ACRONYM(S)
	11. SPONSOR/MONITOR'S REPORT NUMBER(S)

12. DISTRIBUTION/AVAILABILITY STATEMENT

Approved for public release; distribution is unlimited.

13. SUPPLEMENTARY NOTES

14. ABSTRACT

Rapid absorption of impulses using light-weight, small, reusable systems is a challenging problem. An axially aligned set of progressively shrinking elastic spheres, a "tapered chain," has been shown to be a versatile and scalable shock absorber in earlier simulational, theoretical, and experimental works by several authors. We have recently shown (see R. L. Doney and S. Sen, Phys. Rev. Lett. **97**, 155502 (2006)) that the shock absorption ability of a tapered chain can be dramatically enhanced by placing small interstitial grains between the regular grains in the tapered chain systems. Here we focus on a detailed study of the problem introduced in the above mentioned letter, present extensive dynamical simulations using parameters for a titanium-aluminum-vanadium alloy Ti_6Al_4V, derive attendant hard-sphere analyses based formulae to describe energy dispersion, and finally discuss some preliminary experimental results using systems with chrome spheres and small Nitinol interstitial grains to present the underlying nonlinear dynamics of this so-called decorated tapered granular alignment. We are specifically interested in small systems, comprised of several grains. This is because in real applications, mass and volume occupied must inevitably be minimized. Our conclusion is that the decorated tapered chain offers enhanced energy dispersion by locking in much of the input energy in the grains of the tapered chain rather than in the small interstitial grains. Thus, the present study offers insights into how the shock absorption capabilities of these systems can be pushed even further by improving energy absorption capabilities of the larger grains in the tapered chains. We envision that these scalable, decorated tapered chains may be used as shock absorbing components in body armor, armored vehicles, building applications and in perhaps even in applications in rehabilitation science.

15. SUBJECT TERMS

Hertz, granular chain, nonlinear dynamics, anharmonic lattice, 1D lattice

16. SECURITY CLASSIFICATION OF:			17. LIMITATION OF ABSTRACT	18. NUMBER OF PAGES	19a. NAME OF RESPONSIBLE PERSON Robert Doney
a. REPORT	b. ABSTRACT	c. THIS PAGE			19b. TELEPHONE NUMBER *(Include area code)*
Unclassified	Unclassified	Unclassified	UU	20	410-278-7309

Energy partitioning and impulse dispersion in the decorated, tapered, strongly nonlinear granular alignment: A system with many potential applications

Robert L. Doney,[1,a)] Juan H. Agui,[2,b)] and Surajit Sen[3,c)]

[1]*U.S. Army Research Laboratory, Aberdeen Proving Grounds, Maryland 21005, USA*
[2]*NASA-Glenn Research Center, 21000 Brookpark Road, Cleveland, Ohio 44135, USA*
[3]*Department of Physics, State University of New York, Buffalo, New York 14260-1500, USA*

Rapid absorption of impulses using light-weight, small, reusable systems is a challenging problem. An axially aligned set of progressively shrinking elastic spheres, a "tapered chain," has been shown to be a versatile and scalable shock absorber in earlier simulational, theoretical, and experimental works by several authors. We have recently shown (see R. L. Doney and S. Sen, Phys. Rev. Lett. **97**, 155502 (2006)) that the shock absorption ability of a tapered chain can be dramatically enhanced by placing small interstitial grains between the regular grains in the tapered chain systems. Here we focus on a detailed study of the problem introduced in the above mentioned letter, present extensive dynamical simulations using parameters for a titanium-aluminum-vanadium alloy Ti_6Al_4V, derive attendant hard-sphere analyses based formulae to describe energy dispersion, and finally discuss some preliminary experimental results using systems with chrome spheres and small Nitinol interstitial grains to present the underlying nonlinear dynamics of this so-called decorated tapered granular alignment. We are specifically interested in small systems, comprised of several grains. This is because in real applications, mass and volume occupied must inevitably be minimized. Our conclusion is that the decorated tapered chain offers enhanced energy dispersion by locking in much of the input energy in the grains of the tapered chain rather than in the small interstitial grains. Thus, the present study offers insights into how the shock absorption capabilities of these systems can be pushed even further by improving energy absorption capabilities of the larger grains in the tapered chains. We envision that these scalable, decorated tapered chains may be used as shock absorbing components in body armor, armored vehicles, building applications and in perhaps even in applications in rehabilitation science. © *2009 American Institute of Physics.*
[doi:10.1063/1.3190485]

I. INTRODUCTION

There is a recognized need for shock and impulse mitigation in a variety of situations. Common examples in the context of armed conflicts are, for instance, in constructing vests and vehicle surfaces that may be able to withstand bullet impacts and impacts of other more energetic entities.[1] Other examples include impact absorption during controlled explosions, in the context of the aerospace and automobile industries, in protecting structures against seismic shocks and other impacts,[2] in protecting the walls of space crafts from small but fast moving objects in space,[3] and in areas such as in rehabilitation science and technology where cushioning the process of transporting critically injured patients may be necessary and perhaps can be aided by the use of granular chain shock absorbers in the legs.[4]

Here we build on our earlier work[5–11] to develop the broader physics and nonlinear dynamics issues associated with the so-called tapered granular chains, which can serve as key constituents in systems designed for impulse dispersion. It may be noted here that shock absorption capability in the context of armor applications is sometimes captured using "specific absorbed energy" (in units of J/g) or by "gravimetric absorbed energy" (in units of J/cm^3) defined as the difference between the incident kinetic energy on a system and kinetic energy that is transmitted through the system divided by the system mass (for specific absorbed energy) or volume (for gravimetric absorbed energy) (see, for instance, Refs. 12 and 13). In an earlier report we have estimated the projected specific absorbed energy of a plate with embedded tapered chains (TCs) made using titanium-aluminum-vanadium alloys if one were to be constructed. Our estimates suggest that the specific absorbed energy is likely to be in the window of $10^0 – 10^2$ J/g, which would be in the range where several competitive shock absorption technologies would currently find themselves in Ref. 14.

An impulse that is incident on some surface can be characterized by the energy it carries and the duration it lasts. In this work we shall consider impulses that have short enough durations such that they can be characterized by δ-function events. Studies show that impact events that last sufficiently long can lead to unexpected breathing-type dynamics in granular chains.[15,16] Such cases will be addressed separately. The energies of interest are assumed to be such that the impulse can propagate through a set of metallic grains without

a)Electronic mail: bdoney@arl.army.mil.
b)Electronic mail: juan.h.agui@nasa.gov.
c)Electronic mail: sen@dynamics.physics.buffalo.edu.

significantly deforming them so much that they can soften, melt, and/or crack. If we assume that the grains are metallic, this means that we are talking about impulses that are much less than some 10^3 m/s, the latter being the typical sound speed inside a metal. Thus, we shall stay away from considering the direct consequences of typical impulses associated with bullets and projectiles, although indirect impulses caused by such objects may be addressed by the systems we devote this work to. This is not to say that our systems cannot be applied for such large scale impulse mitigation at all but rather that we are not yet in a position to reliably model such impacts on our systems. We have indeed studied the dynamics of our systems at impulses approaching speeds ~750 m/s and preliminary analyses using state of the art hydrocodes[17] indicate that deformations notwithstanding, such impacts may be sustained by our systems.[9] In this work, we interchangeably refer to shocks and impulses, ignoring formal definitions. Since we use a particularly hard and strong material we typically use impact speeds of ~10 m/s. This is somewhat higher than the often used several m/s speeds when using steel balls (see, for example, Ref. 18). Details of the impact speed aside, the crucial point to note is that we assume that for our material of interest the elastic deformation of the grain due to the collision is small enough such that the Hertz law is respected. Indeed it has been observed that for certain materials Hertz theory works surprisingly well up to unexpectedly large impact speeds.[19]

A. The tapered chain and its dynamics

We present here a shock absorbing, one-dimensional (1D) dynamical system[5,7,8] consisting of axially aligned elastic spheres of progressively smaller radii—or a TC. Let us call this system a simple TC (STC). This system is typically assumed to be comprised of metallic grains and disperses incident impulses by spreading them out in time and space through inertial mismatches between the nearest neighbors. The effect was validated experimentally by Nakagawa et al.[6] and by Melo et al.[10] However, such STCs have limited energy dispersion capability when the number of grains is small (say <15). Herein we report overcoming that challenge by introducing smaller beads of constant radius between the grains. These systems, now referred to as decorated TCs (DTCs), represent a significant improvement and turn out to be strongly nonlinear in their dynamical response to impulses.[11] We discuss the results of a preliminary experimental study which confirms that the DTCs are capable of breaking down impulses more efficiently than a STC.

To model such systems, a potential is chosen which emulates an elastic compression—namely, the Hertz potential.[20,21] This strongly, nonlinear function is purely repulsive and is initially softer than a harmonic or Hookean term as two adjacent grains begin to get squeezed. However the potential builds up nonlinearly with progressive compression. The nature of this growth in the potential as the grain-grain distance decreases is measured via the overlap parameter $\delta_{i,i+1}$, where i and $i+1$ denote any two adjacent grains and $\delta_{i,i+1}$ equals the difference between the centers of the adjacent grains when they are squeezed and are barely

touching.[20] Thus, overlap is a positive definite quantity. In the absence of contact, $\delta_{i,i+1}=0$. The nonlinear growth of the Hertz potential in terms of $\delta_{i,i+1}$ is sensitive to the nature of the interface associated with the grain-grain contact.[20] For contacts between spheres, the potential grows as $\delta_{i,i+1}^{5/2}$.

When the grains are all the same size, or monodispersed, any impulse imparted at one end develops into a propagating solitary wave (SW). This has been demonstrated experimentally, numerically, and analytically.[22–31] An approximate analytic estimate of the SW width, w_s, placed its value at five grain diameters.[22,28] Subsequent numerical studies reported it to be closer to seven.[16] When the particles shrink in size by a constant factor, or are polydispersed, a SW cannot form due to translational symmetry breaking at every grain-grain contact.[46] The more massive particle conveys a part of its kinetic energy to the smaller neighbor, which moves faster but carries less kinetic energy. In this manner, tapering allows for progressive breakdown of an impulse and this is what we mean by impulse dispersion in these TC systems.[5] Thus, STCs can be classified as shock dispersion systems or shock "absorbers." The efficiency of these shock absorbers can be shown to increase exponentially with the number of particles, N, and sigmoidally with tapering, q. Their properties have been studied in detail, first numerically,[5,8] then approximately analytically,[5,8] and then experimentally.[6,10] Impulse decimation can also be accomplished by tuning material properties as elucidated by Hong.[32] In fact, this was reported experimentally by Daraio et al.,[33] Fraternali et al.,[34] and Carretero-Gonzalez et al.[35] The dynamics of short chains, $N<10$, have not yet been investigated thoroughly.

These 1D systems have diverse, scalable, and tunable properties. By analyzing the energy transport mechanism, the "ensemble" of systems can be loosely categorized into three groups: SW bearing systems, shock absorption systems, and strongly oscillating systems, where the distinctions are drawn based on how total system energy ends up being partitioned. An intriguing question can be asked: How does the system respond when $N<w_s$ or $N\sim w_s$? These are conditions where the group energy transport mechanism has been interrupted by the boundaries. The boundary, a wall, or sphere of infinite radius obeys a slightly altered potential than that between neighboring grains. Results suggest that with the proper mix of q and $N<w_s$, one obtains quasiperiodic and, possibly, nonlinear modal behavior.

B. Interstitials grains and the decorated tapered chain

An analysis of STCs clearly demonstrated that the best energy dispersion occurs for highly TCs where there are a large number of spheres.[5] Unfortunately, large values of N may not be realizable for many applications where space is at a premium. The natural scalability may be used to drive the system to smaller sizes, but manufacturing issues may become restrictive.[36] Moreover while precompressing the chain can further increase the amount of absorption,[7] that condition needs to be externally maintained throughout the dynamics. Additionally, this pressurized container may pose a safety risk under certain circumstances. How does one then apply short TCs where substantial energy mitigation is needed?

STC: N=11, q=5%

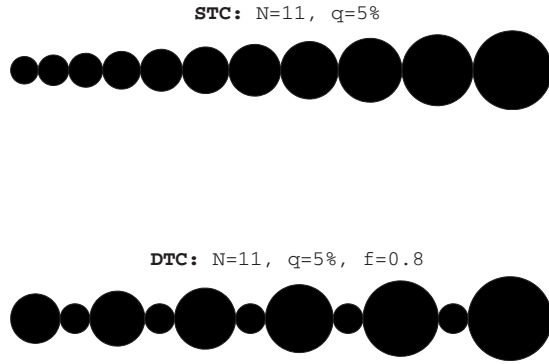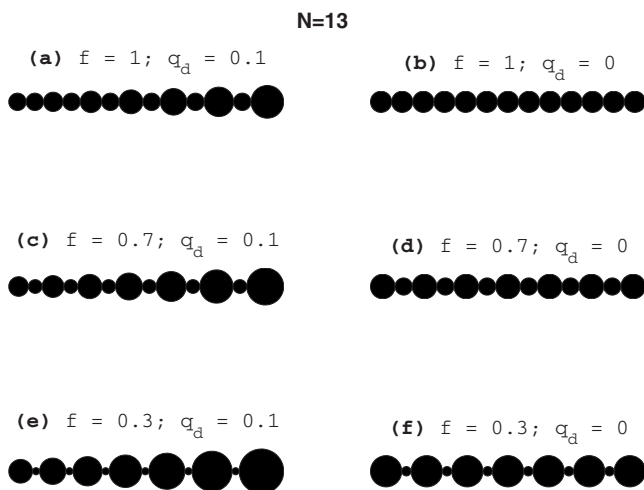

DTC: N=11, q=5%, f=0.8

FIG. 1. An example STC and DTC.

Larger and more frequent inertial mismatches lead to better momentum traps and energy dispersion (see Fig. 1). We therefore proposed a TC system in which we place interstitial grains at the particle contacts of a STC.[11] We refer to this as the DTC (examples shown in detail later in Fig. 2).

As we shall see, the TC systems represent an alternative to current *passive* technologies of dealing with undesirable transients, such as ballistic shock or strong impacts. One such technology uses metal foams and honeycombs.[37,38] When honeycombs are extruded, one obtains a linear cellular alloy,[39] which promises significant energy absorption capabilities.[37] Another approach to impulse dissipation is through the use of functionally graded materials[40] where one can introduce impedance mismatches gradually or discontinuously. What TCs offer as an improvement to currently available technologies is an inherent scalability, the potential for improved performance because of the large parameter space associated with materials used, and a modest if not low cost.[36]

The paper is organized as follows. In Sec. II, a mathematical description of the problem is presented. Hard sphere approximations for both systems follow in Sec. III. Section IV outlines the numerical approach and results for the decorated chain. Section V follows with an analysis of energy partitioning for the two systems and Sec. VI presents preliminary experimental results to establish that our simulational work is qualitatively consistent with the experiments.

N=13

(a) f = 1; q_d = 0.1

(b) f = 1; q_d = 0

(c) f = 0.7; q_d = 0.1

(d) f = 0.7; q_d = 0

(e) f = 0.3; q_d = 0.1

(f) f = 0.3; q_d = 0

FIG. 2. Variety of DTCs possible by varying f and q for constant N=13.

We close in Sec. VII with a summary of the work presented here and remarks about the challenges that lie ahead in constructing systems with embedded TC shock dispersion systems.

II. PROBLEM SETUP

Figure 1 illustrates an example STC (upper panel) and DTC (lower panel). Such chains are parametrized by the number of particles, N, and the amount of tapering, q. The DTC is a STC where an additional particle has been inserted at each particle-particle contact. The particle-boundary interface is unchanged. If the smallest noninterstitial particle at an edge in a DTC has radius, R_N, the interstitial grain is defined as having radius, fR_N. We take the interstitial particle as small ($f<1$) for energy absorption applications. The relation, fR_N, was chosen for convenience for deriving the hard-sphere approximation below. The DTC therefore has the additional parameter f, and has odd N. From this point on, q appears in both STCs and DTCs but is defined differently. For the STC, bead radii are given as

$$R_{i+1}/R_i = 1 - q_s \equiv \epsilon_s, \tag{1}$$

while for the DTC it is

$$R_{i+2}/R_i = 1 - q_d. \tag{2}$$

As such they are denoted as q_s and q_d, respectively. Figure 2 gives a sense of the wide variety of DTC systems possible given f, q_d, and N. It is immediately clear that the inertial mismatch changes as a function of position along the DTC—a dynamic not present for the STC.[8] It is possible then to have decorated chains that appear monodispersed for only a part of the chain (left side of chain in Fig. 2(a) for example).

III. HARD SPHERE APPROXIMATIONS

A. STC

We can quantify the shock absorption efficiency of such chains by measuring the normalized kinetic energy, $K_{norm} \equiv K_{out}/K_{in}$, where K_{in} is the initial impulse energy delivered by the first sphere and K_{out} is the kinetic energy felt by the last sphere due to the first wave front (reflections are neglected). A study assuming that the grain-grain interactions are infinitely stiff (i.e., in the hard-sphere limit)[8] can be carried out to develop an expression for the kinetic energy of the last grain in the STC. In this limit, one can use the energy and linear momentum conservation laws at each grain-grain interaction. The calculation for the STC case has been carried out in earlier work.[8] The momentum and energy conservation conditions can be written as

$$v_i = v_i' + \epsilon_s^3 v_{i+1}' \tag{3}$$

and

$$v_i^2 = v_i'^2 + \epsilon_s^3 v_{i+1}'^2, \tag{4}$$

respectively, and yield $v_{i+1}'/v_i = 2/(1+\epsilon_s^3)$. This result can be now used to derive the final result below,
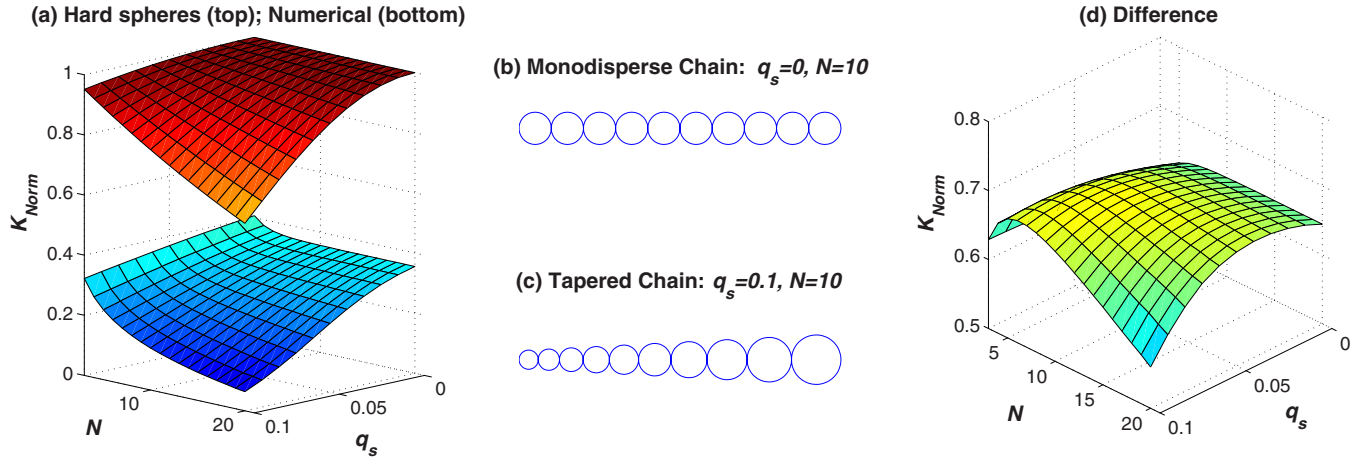
(a) Hard spheres (top); Numerical (bottom)

(d) Difference

(b) Monodisperse Chain: $q_s=0$, $N=10$

(c) Tapered Chain: $q_s=0.1$, $N=10$

FIG. 3. (Color online) (a) Hard sphere approximation and numerically solved normalized kinetic energy surfaces, $K_{norm} \equiv K_{out}/K_{in}$, for the STC as functions of the number of spheres, N, and tapering, q_s. Their difference is plotted in panel (d) with a reduced z-axis. Sample TCs are identified in panels (b) and (c). Reproduced from Fig. 1 in R. Doney and S. Sen, Phys. Rev. Lett. **97**, 155502 (2006). Copyright © 2006 by the American Physical Society (Ref. 11).

$$K_{norm}^{(STC)} = \left(\frac{4(1-q_s)^3}{[1+(1-q_s)^3]^2} \right)^{N-1}. \tag{5}$$

This function is plotted in Fig. 3(a) (top surface). The lower surface is obtained from numerical calculations. Comparison of upper and lower surfaces in Fig. 3(a) reveal that the qualitative characteristics of how $K_{norm}^{(STC)}$ behaves as functions of N and q obtained via the hard-sphere approximation and dynamical simulations are quite close, i.e., $K_{norm}^{(STC)}$ decays exponentially with N and sigmoidally with q in both. The magnitude of $K_{norm}^{(STC)}$ differs between the two (Fig. 3(d). It turns out that this difference is because in the hard-sphere approximation treatment, the contribution of the potential energy is set to zero and all the energy is regarded as kinetic. In a real system, some 44.5% of the total energy is potential energy.[7,41,42] Thus the magnitude of the kinetic energy that is transported through the system is much less. Once the value of $K_{norm}^{(STC)}$ in the hard-sphere calculations is multiplied by 0.555, the agreement between the two studies improves significantly as long as we restrict ourselves to sufficiently long and TCs. The departure between the results obtained through the two approaches are largest for chains that are sufficiently small and are not appropriately tapered. We shall later see that this departure arises from the nonlinear effects associated with the Hertz potential.[43] We shall return to a discussion of these issues in Sec. IV. As we shall see in this work, such a simple minded "renormalization" does not bring the hard-sphere based and dynamical simulation based analyses into close agreement for the DTC case. Moreover this is why we must regard the dynamics of the DTC as intrinsically nonlinear in nature where the potential energy of the grains plays a rich role in its dynamics.

B. DTC

In deriving an approximation for the DTC, the process is more cumbersome and the conservation equations for mass and energy are successively applied to obtain the grain velocities until a pattern emerges. Our primary interest is in deriving an expression for the normalized kinetic energy,

$$K_{norm} = \frac{K_{out}}{K_{in}} = \frac{m_N}{m_1} \left(\frac{v_N'}{v_1} \right)^2 = \frac{m_N}{m_1} \left\{ \left(\frac{v_N'}{v_{N-1}'} \right) \cdots \left(\frac{v_{i+2}'}{v_{i+1}'} \right) \right.$$
$$\left. \times \left(\frac{v_{i+1}'}{v_i'} \right) \cdots \left(\frac{v_2'}{v_1} \right) \right\}^2. \tag{6}$$

We will eventually look for forms of v_{i+1}'/v_i and then generalize for N particles or $(N-1)$ collisions. First, the relationship among masses and radii must be evaluated. Assembling the radii, we have starting with the largest bead,

$$r_i,$$

$$r_{i+1} = fr_N,$$

$$r_{i+2} = r_i - qr_i = (1-q)r_i = \epsilon r_i,$$

$$r_{i+3} = fr_N,$$

$$r_{i+4} = r_{i+2} - qr_{i+2} = (1-q)r_{i+2} = \epsilon^2 r_i,$$

$$r_{i+5} = fr_N,$$

$$r_{i+6} = r_{i+4} - qr_{i+4} = (1-q)r_{i+4} = \epsilon^3 r_i,$$

$$\vdots$$

$$r_{N-1} = fr_N,$$

$$r_N = r_{N-2} - qr_{N-2} = (1-q)r_{N-2} = \epsilon^{(N-1)/2} r_i.$$

The main equations for radii are therefore

$$r_N = \epsilon^{(N-1)/2} r_i,$$

$$r_{(i+1),(i+3),\ldots,(N-1)} = f\epsilon^{(N-1)/2} r_i. \tag{7}$$

Recall for masses that $m_i = \rho V_i = \frac{4}{3}\pi r_i^3 \rho = \eta r_i^3$. Note that since η is just a constant and will cancel once the conservation equations are set into use, we will ignore it from now on. Expressions for m_i then become

$$m_i \sim \epsilon^0 r_i^3,$$

$$m_{i+1} \sim r_{i+1}^3 = A r_i^3,$$

$$m_{i+2} \sim \epsilon^3 r_i^3,$$

$$m_{i+3} \sim r_{i+3}^3 = A r_i^3,$$

$$m_{i+4} \sim \epsilon^6 r_i^3,$$

$$\vdots$$

$$m_{N-1} \sim r_{N-1}^3 = A r_i^3,$$

$$m_N \sim \epsilon^{3(N-1)/2} r_i^3, \tag{8}$$

where $A = f^3 \epsilon^{3(N-1)/2}$. We may now use these relations to set up the conservation equations. Beginning with momentum and assuming that each subsequent particle in the chain begins at rest, we solve for the first five collisions. Primes and double primes indicate postcollision states. A primed quantity denotes the first postcollision state of a sphere. That subsequent sphere will serve as the input to the next collision. To keep track of its velocity after the second collision, it is denoted by a double prime and will eventually be eliminated. With $\epsilon = (1-q)$, we obtain

$$m_i v_i = m_i v_i' + m_{i+1} v_{i+1}' \rightarrow v_i = v_i' + A v_{i+1}', \tag{9}$$

$$m_{i+1} v_{i+1}' = m_{i+1} v_{i+1}'' + m_{i+2} v_{i+2}' \rightarrow A v_{i+1}' = A v_{i+1}'' + \epsilon^3 v_{i+2}', \tag{10}$$

$$m_{i+2} v_{i+2}' = m_{i+2} v_{i+2}'' + m_{i+3} v_{i+3}' \rightarrow \epsilon^3 v_{i+2}' = \epsilon^3 v_{i+2}'' + A v_{i+3}', \tag{11}$$

$$m_{i+3} v_{i+3}' = m_{i+3} v_{i+3}'' + m_{i+4} v_{i+4}' \rightarrow A v_{i+3}' = A v_{i+3}'' + \epsilon^6 v_{i+4}', \tag{12}$$

$$m_{i+4} v_{i+4}' = m_{i+4} v_{i+4}'' + m_{i+5} v_{i+5}' \rightarrow \epsilon^6 v_{i+4}' = \epsilon^6 v_{i+4}'' + A v_{i+5}',$$
$$\vdots \tag{13}$$

From the pattern in Eqs. (9)–(13), Eq. (9) can be rewritten as $\epsilon^0 v_i' = \epsilon^0 v_i' + A v_{i+1}'$. An evaluation of energy conservation yields the same form as Eqs. (9)–(13) except velocities are squared,

$$v_i^2 = v_i'^2 + A v_{i+1}'^2, \tag{14}$$

$$A v_{i+1}'^2 = A v_{i+1}''^2 + \epsilon^3 v_{i+2}'^2, \tag{15}$$

$$\epsilon^3 v_{i+2}'^2 = \epsilon^3 v_{i+2}''^2 + A v_{i+3}'^2, \tag{16}$$

$$A v_{i+3}'^2 = A v_{i+3}''^2 + \epsilon^6 v_{i+4}'^2, \tag{17}$$

$$\epsilon^6 v_{i+4}'^2 = \epsilon^6 v_{i+4}''^2 + A v_{i+5}'^2,$$
$$\vdots \tag{18}$$

We can combine Eqs. (9)–(18) to eliminate the double-primed terms and form the velocity ratios: v_{i+1}'/v_i, v_{i+2}'/v_{i+1}', etc. Beginning with Eq. (9), we isolate v_i' and square to

obtain $v_i'^2 = v_i^2 - 2A v_i v_{i+1}' + a^2 v_{i+1}'^2$. Next substitute this into Eq. (14) and rearrange to obtain v_{i+1}'/v_i. This is then repeated for Eqs. (10), (15), (11), and (16) to obtain the following ratios:

$$\frac{v_{i+1}'}{v_i} = \frac{2\epsilon^0}{A + \epsilon^0}, \tag{19}$$

$$\frac{v_{i+2}'}{v_{i+1}'} = \frac{2A}{\epsilon^3 + A}, \tag{20}$$

$$\frac{v_{i+3}'}{v_{i+2}'} = \frac{2\epsilon^3}{A + \epsilon^3}, \tag{21}$$

$$\frac{v_{i+4}'}{v_{i+3}'} = \frac{2A}{\epsilon^6 + A}, \tag{22}$$

$$\vdots$$

where hindsight has allowed us to insert terms of ϵ^0 in Eq. (19). With our eye fixed on Eq. (6), results may be merged. Thus

$$\frac{v_N'}{v_1} = \left(\frac{v_2'}{v_1}\right) \cdots \left(\frac{v_{i+1}'}{v_i}\right)\left(\frac{v_{i+2}'}{v_{i+1}'}\right) \cdots \left(\frac{v_N'}{v_{N-1}'}\right), \tag{23}$$

$$= \underbrace{\underbrace{\left(\frac{2\epsilon^0}{A+\epsilon^0}\right)\left(\frac{2A}{\epsilon^3+A}\right)}_{N=3}\left(\frac{2\epsilon^3}{A+\epsilon^3}\right)\left(\frac{2A}{\epsilon^6+A}\right)}_{N=5}\left(\frac{2\epsilon^6}{A+\epsilon^6}\right)\left(\frac{2A}{\epsilon^9+A}\right)}_{N=7}, \tag{24}$$

The ratio can be placed into closed form to obtain

$$\therefore \frac{v_N'}{v_1} = \prod_{j=1}^{(N-1)/2} \left(\frac{2\epsilon^{3(j-1)}}{A + \epsilon^{3(j-1)}}\right)\left(\frac{2A}{\epsilon^{3j} + A}\right),$$

$$= 2^{N-1} A^{(N-1)/2} \prod_{j=1}^{(N-1)/2} \left(\frac{\epsilon^{3(j-1)}}{A + \epsilon^{3(j-1)}}\right)\left(\frac{1}{\epsilon^{3j} + A}\right). \tag{25}$$

Turning to the mass ratios and using expressions from Eq. (8), it turns out that most terms cancel,

$$\frac{m_N}{m_1} = \left(\frac{m_2}{m_1}\right) \cdots \left(\frac{m_{i+1}}{m_i}\right)\left(\frac{m_{i+2}}{m_{i+1}}\right) \cdots \left(\frac{m_N}{m_{N-1}}\right),$$

$$= \left(\frac{A}{\epsilon^0}\right)\left(\frac{\epsilon^3}{A}\right)\left(\frac{A}{\epsilon^3}\right)\left(\frac{\epsilon^6}{A}\right) \cdots,$$

leading to the simple expression

$$\frac{m_N}{m_1} = \epsilon^{3(N-1)/2}. \tag{26}$$

We can now identify the normalized kinetic energy in Eq. (6) by squaring Eq. (25) and combining it with Eq. (26) to form
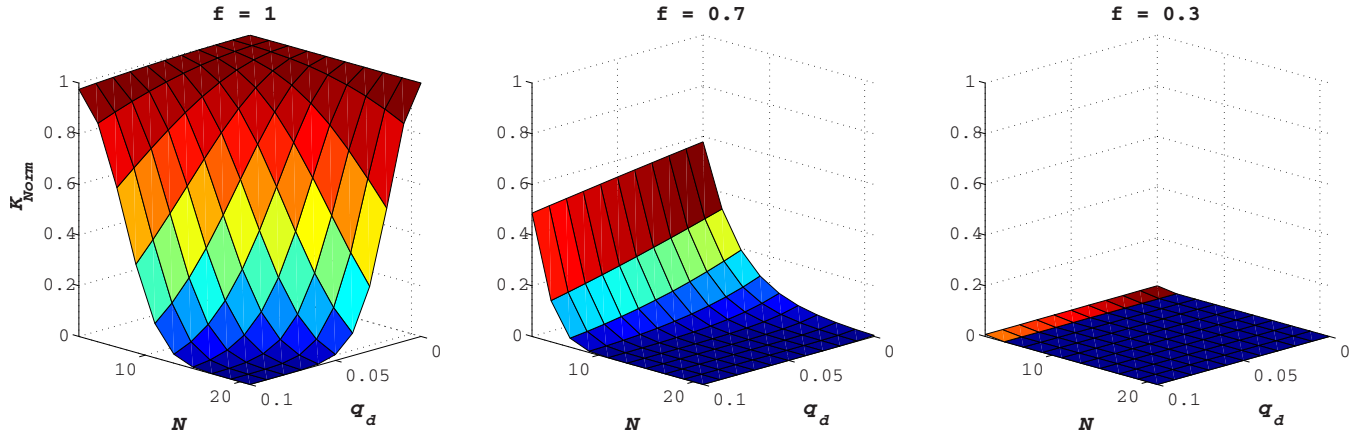
FIG. 4. (Color online) Normalized kinetic energy surfaces, $K_{norm} \equiv K_{out}/K_{in}$, for the decorated chain under the hard-sphere approximation as functions of the number of spheres, N, fractional size of interstitial sphere, f, and tapering, q_d. Reproduced from Fig. 2 in R. Doney and S. Sen, Phys. Rev. Lett. **97**, 155502 (2006). Copyright © 2006 by the American Physical Society (Ref. [11]).

$$K_{norm}^{(DTC)} = (4A\epsilon^{3/2})^{(N-1)} \left\{ \prod_{j=1}^{(N-1)/2} \frac{\epsilon^{3(j-1)}}{(A + \epsilon^{3(j-1)})(\epsilon^{3j} + A)} \right\}^2.$$

(27)

These results are plotted in Fig. 4. The effects of the interstitial sphere are remarkable when compared to the STCs in Fig. 3(a) (top surface). For a modest value, $f=0.7$, it takes very few particles to reduce the outgoing kinetic energy considerably.

It is difficult to draw any physical intuition from Eq. (27). However, a very curious and astonishing result occurs in the limit $q_d=0$,

$$K_{norm}^{(DTC)} \Big|_{q_d=0} = \left(\frac{4f^3}{[f^3 + 1]^2} \right)^{N-1}.$$

(28)

This limit is equivalent to Eq. (5) under the exchange $f \Leftrightarrow (1-q_s)$.

As a result, K_{norm} decays as a half Gaussian or sigmoid with increasing f, and exponentially with increasing N. It is clear that $f=1$ should imply $q_s=0$ since they both generate monodisperse chains. That this equivalency goes beyond that special case is quite unexpected. One can now begin to see the significant effect f has on the energy mitigation capability when an infinite potential is invoked: For $f=0.3$—a typical value we might consider—the equivalent tapering in the STC would be $q_s=0.7$. This value is seven times larger than any system we had previously considered and could be a significant system integration challenge. For hard spheres, the energy mitigation capability of the STC shown in Fig. 1 (top) (but $q_s=1\%$) is identical to that for a decorated chain similar to that shown in Fig. 1 (bottom) but with $q_d=0$, $N=10$, $f=0.9$.

IV. NUMERICAL SOLUTION

The spheres can be assumed to interact through the strongly nonlinear Hertz potential,[20,21]

$$V(\delta_{i,i+1}) = \frac{2}{5D}\sqrt{R_i R_{i+1}/(R_i + R_{i+1})}\, \delta_{i,i+1}^{5/2} \equiv a_{i,i+1}\delta_{i,i+1}^{5/2},\quad (29)$$

where $\delta_{i,i+1}=R_i+R_{i+1}-(z_{i+1}-z_i)$ represents the overlap of successive grains and z_j is the absolute position of a grain. The constant $D \equiv 3/2[(1-\sigma^2)/E]$, where E and σ describe Young's modulus and Poisson's ratio of the material, respectively. We have used the material properties of Ti_6Al_4V for our studies and for this material Young's modulus, $E=114$ kN/mm^2, and Poisson ratio, $\sigma=0.33$. In addition, for each chain, an initial velocity of 0.01 mm/μs (10 m/s) is applied to the largest grain.[44] Our numerical approach uses the velocity-Verlet[45] algorithm with a time step of 10 ps integrated over 10^8 steps. Energy is conserved to about one part in 10^{12}. Results will primarily focus on the evaluation of K_{norm} surfaces [Fig. 3(a)]. Restitutive losses are accounted for in the code, however they are excluded in this study. Therefore, since these particulate systems will have several modes of energy dissipation—friction, rolling, slipping, sound, etc., which are simply additive (because work-energy theorem implies that work done by a system in overcoming dissipation necessarily implies kinetic energy loss), these surfaces must represent the worst cases.

It is known that among other constraints, the Hertz potential is valid when impulse speeds are sufficiently less than the sound speed of the material. As mentioned earlier, we have begun hydrocode simulations exploring impact velocities close to 1 km/s, which suggest continued energy absorption well beyond 10 m/s.[17]

The equations of motion for the granular chain where the grain sizes and masses can vary are then given as

$$m_i \ddot{z}_i = \frac{5}{2}\{a_{i-1,i}\delta_{i-1,i}^{3/2} - a_{i,i+1}\delta_{i,i+1}^{3/2}\},$$

(30)

and this general equation has no known analytic solution.

Figure 3 plots the hard-sphere (top surface) and numerical (bottom surface) results for the STC. The reason for the discrepancy between the two solutions is, of course, due to the potential energy part of the total energy which has been ignored in the hard-sphere analyses. For hard spheres, the sequence consists of independent collisions[46] where the velocity ratio is $v_{i+1}/v_i=2/[1+(1-q_s)^3]$. Since the potential is
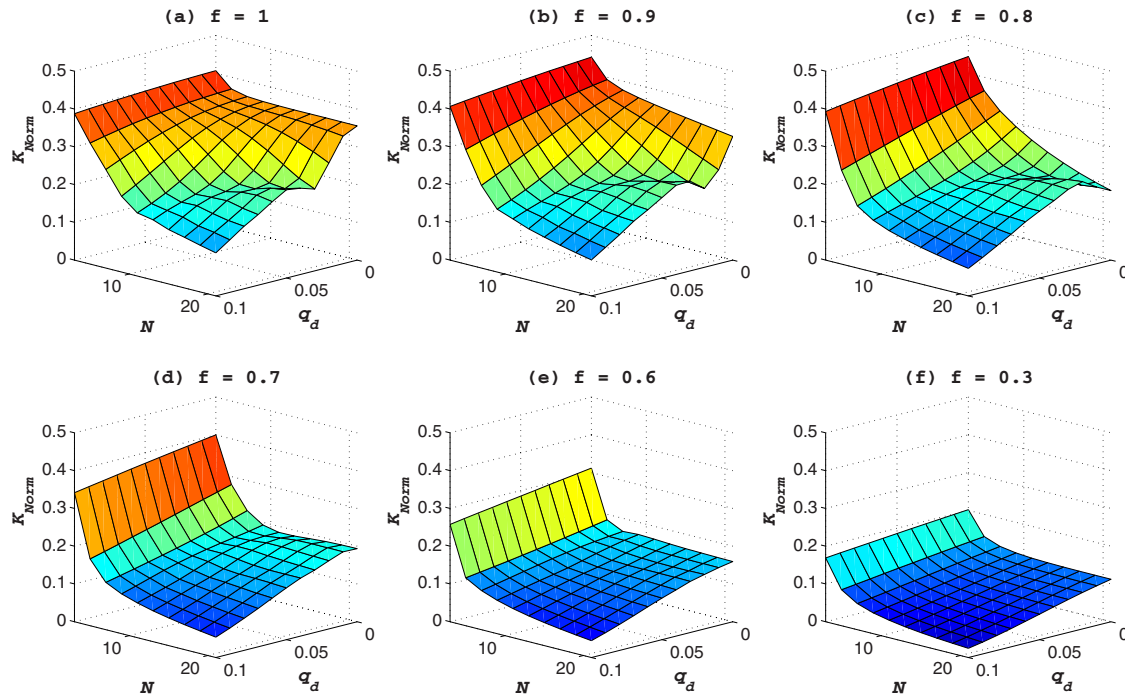
FIG. 5. (Color online) Numerically produced normalized kinetic energy surfaces, $K_{norm} \equiv K_{out}/K_{in}$, for the decorated chain as functions of the number of spheres, N, fractional size of interstitial sphere, f, and tapering, q_d. Several sample chains are identified in panels (d)–(i).

infinite, energy and momentum are transferred instantaneously. Further, the hard spheres are not confined and momentum always carries them *forward* after interacting (presuming $q_s \neq 0$). Numerically, rebounding occurs. Even if $q_s = 0$—i.e., inertial matching—the natural partitioning of energy seen numerically is not accounted for by the approximation. Thus, for hard spheres, all of the energy is kinetic as compared to about 55.5% when the numerical-based analysis is performed. These differences are plotted directly in Fig. 3(d).

Figure 5 highlights the computational results for the decorated chain. Recall that the inertial mismatch between neighboring grains in decorated chains change as a function of position along the chain. This is what we believe to be the cause of a ripple in the surface of the K_{norm} plots that propagate toward the origin as f decreases. As one might expect, such behavior would be functions of N, q_d, and f. The effect vanishes for $f \lesssim 0.6$, approximately. At about this threshold, the interstitial grain is not much smaller (less massive) than the grains toward the end of the chain. The explanation is that as an impulse propagates, energy transmission becomes increasingly efficient due to smaller inertial mismatches—a prerequisite for admitting SWs. Thus the system changes from a shock absorber to shock transmitter. This effect however must compete with compressive effects in some manner since no such behavior is present for hard spheres even though it too has a position-dependent inertial mismatch.

The hard-sphere approximation grossly exaggerates the shock mitigation capability of the decorated chain. Additionally, it does not pick up the surface feature resulting from a competition between particle overlap nonlinearity and variable inertial mismatches between neighboring grains. Simulations suggest that for $f = 0.3$, $N = 5$, $q_d = 0.1$, one can disperse energy within the chain such that only about 10% of

that set into the system is transmitted to the end with the initial pulse. At later times, dissipation sufficiently attenuates the pulse such that only the first trip of the energy from the largest to the smallest grain matters most.

V. ENERGY PARTITIONING

Tracking the partitioning of energy in a many body dynamical system is an effective way to develop insights into its dynamics. For instance, it provides a measure of how much of the system is in motion versus how much is squeezed and how these change in time. Energy information about the whole TC system can be evaluated by summing the kinetic and potential contributions of each bead and allows us to check the accuracy of our calculations. In all cases, we have seen that energy sharing among particles is rapid and remains nonlocalized in the TCs. Here attention is paid to the energetic response of the system (Sec. V A) with some consideration to individual particle velocities (Sec. V B).

A. STC

Energy partitioning in the STC is displayed as 12 subplots in Fig. 6, where each plot element represents a chain with $N = 3, 8, 14, 20$, $q_s = 0, 0.05, 0.1$ for each case of N as labeled in Fig. 6. For clarity, only the first fifth of simulation time is shown. Thereafter the initial pulse is broken down into smaller, disordered pulses. Many interesting features, visible in the plots, can be discussed qualitatively and suggest the three energy regimes ascribed earlier, the most notable of which include frequent and nearly complete energy conversion for small N; organized energy transmission for small q_s, large N; and noisy, disordered behavior for large q_s, large N.
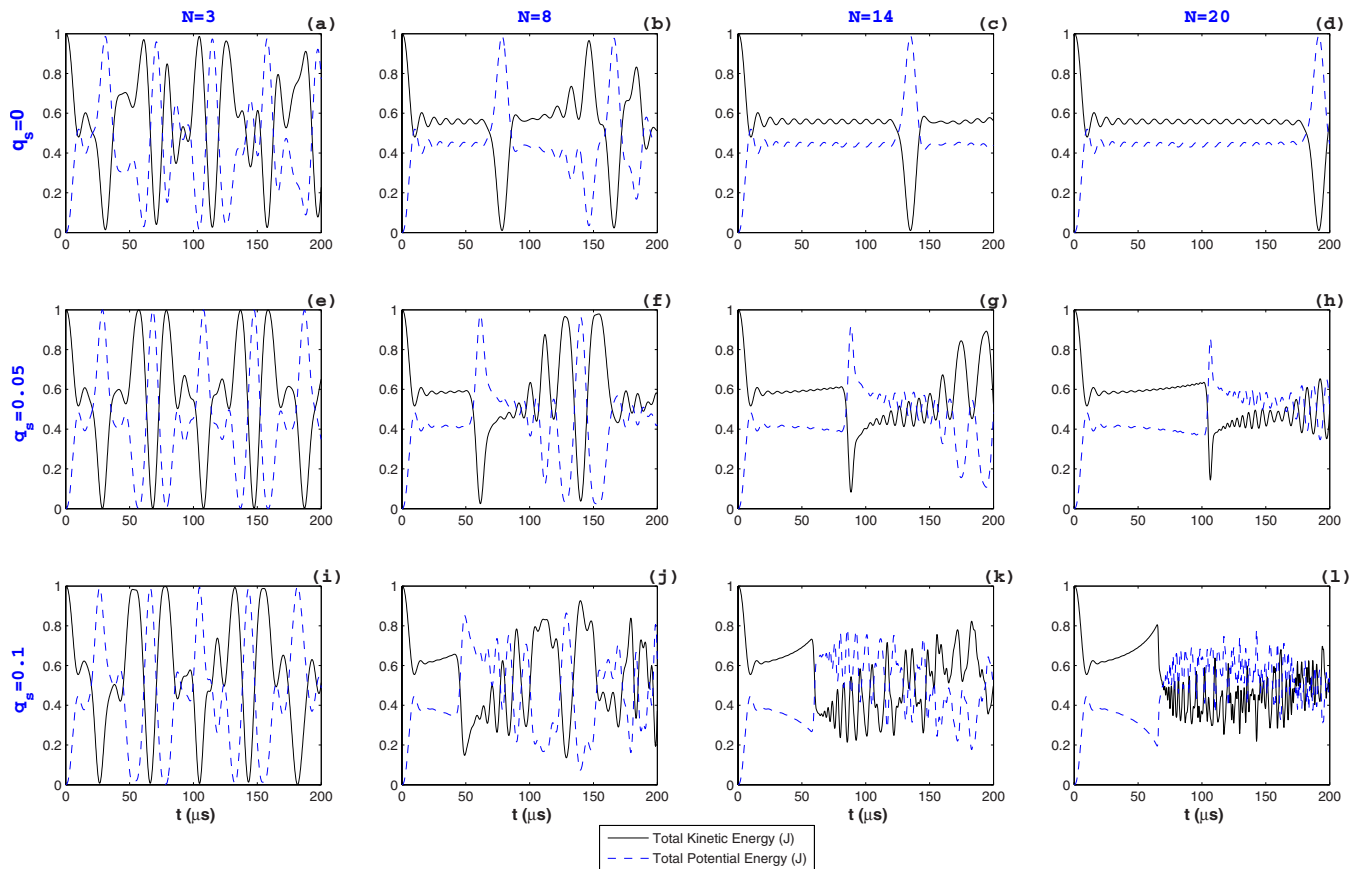
FIG. 6. (Color online) Energy partitioning for STCs where $N=\{3,8,14,20\}$ represents the number of spheres and $q_s=\{0.0,0.05,0.1\}$ is the tapering. Noisy plots resembling panel (l) indicate shock absorbing systems while those similar to panel (j) transmits an impulse as a SW—essentially without loss. Panels (a)–(c) represent efficient energy conversion systems.

The simplest case to consider is that of Fig. 6(d) as it has been studied before[7] and represents a monodisperse chain of 20 grains. It is clear in this instance that energy is partitioned into 55%–56% kinetic and 45%–44% potential. An inspection of grain speeds reveal that the first several particles retain some residual velocity before a SW can form—which also holds true for every plot in the figure (see Fig. 7(a) for example).

Holding $N=14$ fixed and increasing q_s results in faster moving particles as one moves down the chain as well as wave broadening. This is visible in panels (g), (h), (k), and (l) as an increasing ramp whose slope is steeper with increasing q_s and smoothening of the sinusoidal modulations, respectively. Compare this with the wave broadening among multiple grains with increasing q_s seen in Fig. 7. Interaction with the boundary follows and in some cases, the energy envelope increases because most particles have already reversed direction. Close inspection reveals that trailing particles can catch up and kick leading particles into higher energy states. In panels (k) and (l) rapid oscillations, or thermalization, are visible. This is an indication of increasing "randomness"[47,48] of motion and spreading of the energy in time and space—a prerequisite for impulse decimation.

As one moves to shorter chains, where the SW width $w_s > N$ like those in panels (a), (e), and (i), nearly complete conversion of energy frequently takes place. Wave reflection therefore has begun before full transmission of the incident
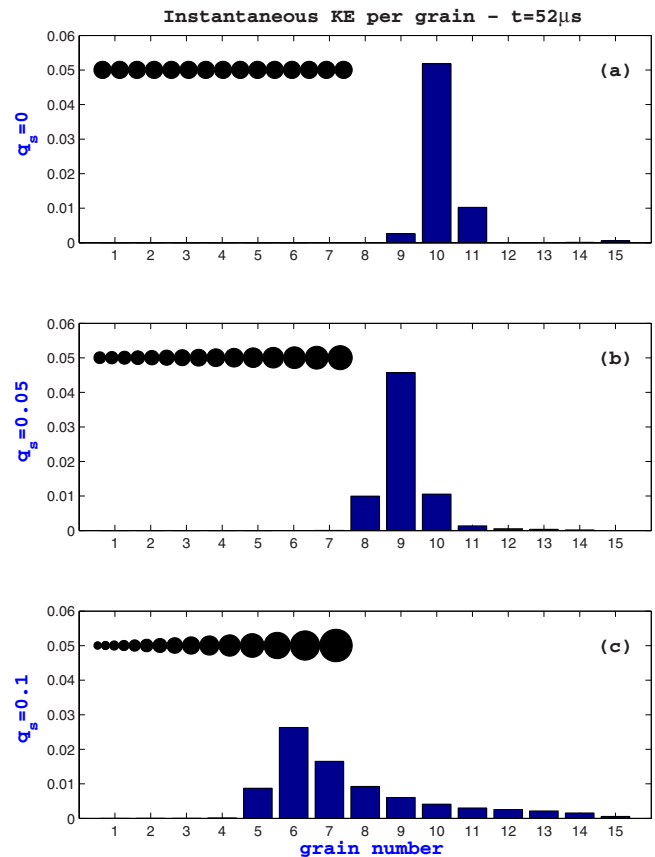

FIG. 7. (Color online) Instantaneous kinetic energy per grain for $N=15$, $t=52$ μs, and selected tapering.
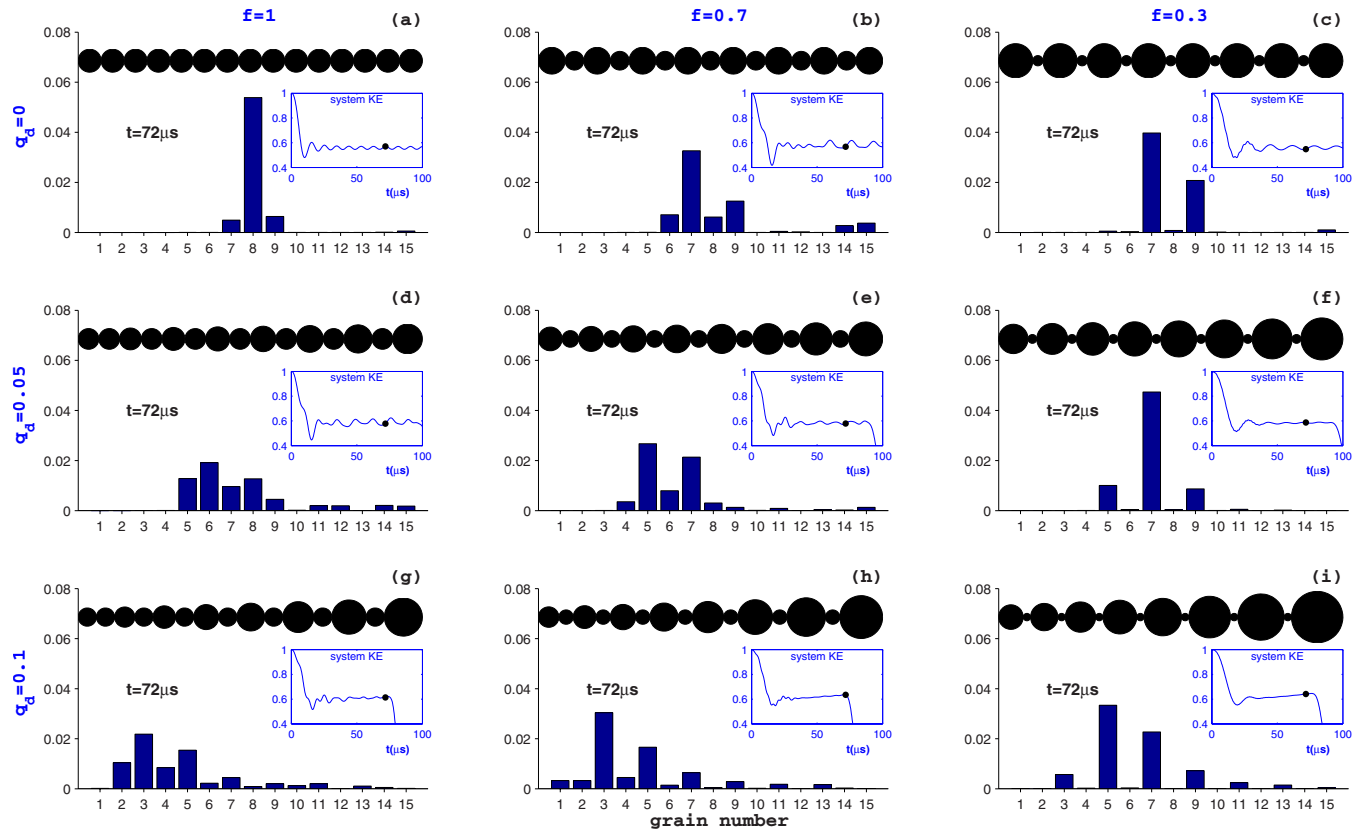
FIG. 8. (Color online) Instantaneous kinetic energy per grain for various DTC configurations at $t=72$ μs, where $q_d=\{0,0.05,0.1\}$ and $f=\{1.0,0.7,0.3\}$.

pulse would normally reach the boundary of a longer chain. Consequently they become "dilated" and large parts of the system can move in phase. Increasing q_s for $N=3$ appears to enhance the energy conversion efficiency. In fact, panel (b) is particularly compelling given its quasiperiodicity. Amplitude of the intermediate weak peaks vary based on q_s and represent energy transfer through the center bead. This behavior throughout the simulation suggests the possibility of nonlinear modes.[49] Consequently, such TCs are not useful for shock absorption since coordinated movement could amplify delivered force. Thus, there may be *limitations to the reduction* that may be possible in the number of grains needed to ensure that a TC is capable of impulse dispersion.

Additionally, one can take a mesoscopic view and investigate how STC systems break down the energy per grain. This is illustrated in Fig. 7 where the instantaneous kinetic energy is plotted per grain for $N=15$, $t=52$ μs, and a selection of tapering values and the incident impulse moves from right to left. In other words, the grain numbers define the energy carried by grains at a fixed instant in time. Panel (a) represents the monodisperse chain and the localization of energy is apparent as the SW is constructed. Recall that it takes between 10 and 15 grains for SWs to be established. Even for inertially matched spheres, some residual energy is left at the head of the chain (right-hand side). Panels (b) and (c) again illustrate the effect of tapering which spreads the energy out among grains. For the latter, the distribution before interacting with a boundary appears geometric. It is clear that a SW cannot exist in such chains.

B. DTC

A simple view of energy partitioning in the DTC is not possible given the vast number of possible chain configurations, belittling those of the STC. Changing N has a much more severe impact on the results because, by design, it affects the results everywhere in the chain. For example, if we take the mass ratio of interstitial grains for $N=21$ and $N=11$ chains, with q_d and f identical, the results scale astonishingly: $m_{N=21}/m_{N=11} \propto (1-q_d)^{15}$! For large tapering, $q_d=0.1$, interstitial grains in a chain with $N=21$ have about one-fifth the mass as their counterparts where $N=11$.

Rather than focusing on the dynamics of the entire system, we focus on how a DTC partitions the energy among particles as an impulse propagates. Our studies suggest that controlled partitioning of energy offers very good ways to absorb and disperse the energy of an impulse.[32,33] Figure 8 illustrates the instantaneous kinetic energy per grain for various configurations at $t=72$ μs, where $q_d=\{0,0.05,0.1\}$ and $f=\{1.0,0.7,0.3\}$ (see the figure labels). The black disk that is visible in the inset indicates the current time for the bins. At this chosen instant, the pulse is just about to hit the end wall and turn around—specifically for $q_d=0.1$. Also included in each panel is a silhouette of the specific chain and the total kinetic energy of the system as a function of time where the pulse is initially moving from right to left. It should be noted that panel (a) is identical to Fig. 7(a)—at different times—since they are both monodisperse chains. A cursory glance of all panels reveal that the effect of q_d is to spread the impulse out over many grains in a manner similar to the STC. Sec-

ond, and somewhat surprisingly, when decreasing f the *energy appears to be preferentially distributed to the larger, noninterstitial* (odd numbered) grains. Hence, in these strongly nonlinear systems, there is no guarantee that a "plasma mode" would be sustainable in the light masses.[50] It is hypothesized that additional, neighboring interstitial spheres would further separate the energy along the chain. What this also appears to do is turn the DTC into, effectively, a binary collision system since the amplitudes of interstitial spheres are quite superficial. It may be of interest to note that the speed of energy transmission appears more strongly dependent on q_d than on f, a property that is evident from Fig. 8. This was an unexpected result to us as we had naively expected that the interstitial grains would perhaps trap energy better than the larger grains of the TC part of the system would.

The division of energy into the larger grains for small f appears to be a result of their larger masses, rather than the increased "rattling" of interstitial spheres. For example, the mass ratio between grains 15 and 14 in Fig. 8, panel (i) is about 0.004. This value becomes more matched as one approaches grains 1 and 2 which has a ratio of about 0.03. Even though the even-numbered grains have a much higher velocity than their larger neighbors, kinetic energy only scales as v^2 versus $m \sim r^3$. The smaller system kinetic energy plots in each panel reveals the complicated nature of the system—a consequence of the competition among f, q_d, N. The dynamics tend to be smoother for small f because of the apparently minor role played by interstitial spheres to the total system energy. When f is sufficiently small, much smaller than the smallest f we have considered here ($f = 0.3$), it is possible that the elastic assumption would become invalid and the plasticity of the smaller interstitial grains would become significant. At this time, there is no simple way to carry out such analysis.

Figure 8 panels (b) and (c), which pertain to $q_d = 0$ and hence monodispersed chain of larger grains, may not necessarily admit SWs but localized energy propagation does occur in these systems, thus raising the possibility of using interstitials to make multiple propagating SWs. The formation of multiple SWs could arise from extended loading times between the interstitial and the larger grains for sufficiently small f (in this context, see Refs. 16 and 51). In both cases, the amplitude dampens, in agreement with Manciu and co-workers[28,52]—this is more obvious with larger N (not pictured). Panels (f) and (i) quickly spread out the energy because of the finite tapering which is also the reason for an increasing KE ramp (shown in the inset). However, tapering q_d now must compete with f as results vary significantly among other panels. A thorough analysis of that rivalry has not yet been investigated.

VI. EXPERIMENTAL SETUP AND RESULTS

A picture of the experimental setup is shown in Fig. 9. A stainless steel V-grooved rail was used to align and retain the granular alignment in contact with the face of the load cell. The V-groove surface was ground to reduce friction on the spherical particles and minimize instantaneous rolling of the
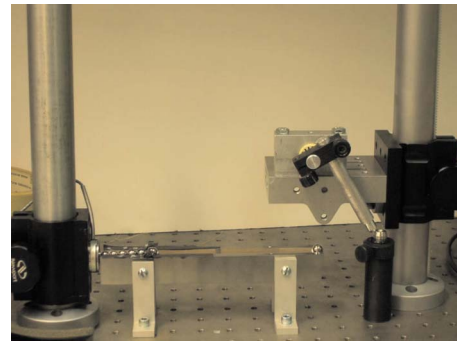

FIG. 9. (Color online) V-groove apparatus with pendulum for the STC experiments.

initially static particles (for a discussion of rolling related issues, see Ref. 6). The spherical particles were chrome steel ball bearings. A simple pendulum impacting mechanism was devised to generate a reproducible impact force and subsequently numerous tests were performed on the impactor to show that it produced a repeatable impact force. The standard deviation in force measurements was less than 1%. The data were recorded on a 16 bit data acquisition package with a 75 dB signal to noise ratio. The force measurement was registered by a 1000 lb compression load cell with a natural resonant frequency of 35 KHz. We used two setups for the studies. The first was a STC in which all particles were in contact along the chain. Both $N=5$ and $N=6$ were used in this configuration. The first and largest particle in the chain had a diameter of 10 mm and the tapering for the subsequent balls was about $5 \pm 1\%$. The second was the DTC setup. In this case, small Nitinol 2.38 mm diameter particles were introduced between the main STC particles so that $N_{DTC}=9$.[53] The difference in chain length between the latter and the STC $N=6$ was only about 2 mm. Placement was crucial for stability of the chain and for the force transmission to take place through the grains. Any collapse of the chain would have significantly altered the force measurement. A close-up of the Nitinol particle placement is shown in Fig. 10. Kevlar thread was glued to two opposing sides of the interstitial particles for anchoring it to the rail using tape. These threads are visible in the image extending into and out of the page. In

FIG. 10. DTC apparatus showing Kevlar thread glued to the interstitial particles.
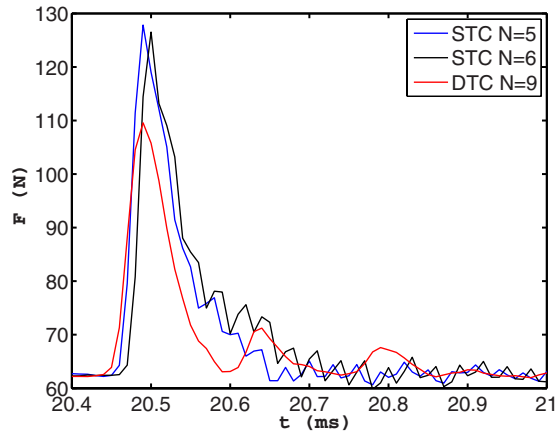
FIG. 11. (Color online) Delivered force for the $N=5,6$ STC and $N=9$ DTC experiments.

FIG. 12. (Color online) Simulations of comparative setup to those in Fig. 11.

the background, one can discern the threads taped to the rail. Time was spent properly aligning the Nitinol particles along the center axis of the chain. High speed video was taken during each run to ensure that the data correlated with a stable chain during impact propagation. The video was recorded on a Photron camera at 1000×1000 pixel resolution at 1000 frames/s. Runs with collapsed chains were not considered in the reduced data.

We performed ten test runs each between the STC and DTC setups. A plot comparing typical impact forces among the five and six particle STCs and the nine particle DTC is presented in Fig. 11. *Impact forces reached close to* 200 N. These plots are quantitatively representative of the remaining plots from each of the other test runs. Notice the slight decrease in force for the six particle STC versus the five particle STC. The additional particle and tapered differences added 7.36 mm to the length of the chain and an additional contact and a mass increase of 11.9%. In comparison, the DTC produced a 25% attenuation in force. Because of the four interstitial Nitinol particles the contacts went up by 4 and the chain length was increased by 9.5 mm, but with only a 1.4% increase in mass. The signal for the DTC shows a more pronounced drop but characteristic in decay as the STC cases. This seems to indicate that for stable chains the rebound was immediate with no sideway motion, at least during the forward impulse direction. For close comparison with simulations it would have been desirable to directly measure grain velocities. However, such measurements are very difficult to perform with reasonable accuracy in these systems at this time.

It is almost impossible to quantitatively *compare* the experimental results on force measurements with simulations in this strongly nonlinear system of Hertz contacts. Some of the challenges associated with modeling are as follows: (i) little is understood about how to accurately model restitutive and frictional losses in these systems (for some recent discussions on this topic see, for example, Refs. 54 and 55), (ii) simulations with an open boundary at the striker end, as in the experiments, pose challenges associated with modeling the effects of rolling, and (iii) there is no *simple* way to simulate the pressure felt by the surface of a force sensor at the tapered end without making a realistic plate in the model
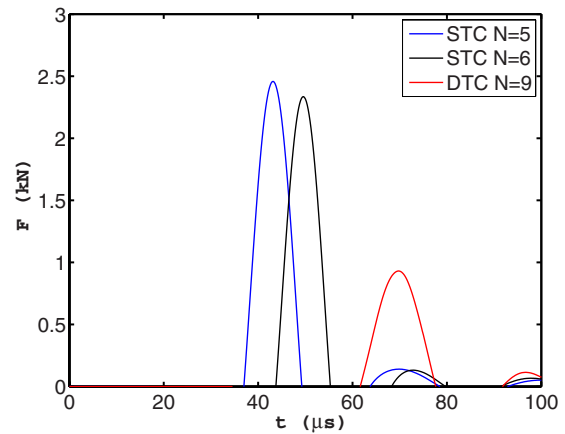
to simulate the wall, which in itself poses major challenges. Nevertheless, we are hopeful that our current studies using hydrocodes would provide some insights into modeling (i) and (iii) above in due course.

Results from simulations for a similar system, as in the experiment, are presented in Fig. 12 where we find that even at higher impact velocities—but remaining within the elastic regime—the experimentally observed trend in delivered force is the same. For simplicity we consider the interstitial grains and the grains in the TC to have the parameters of Ti_6Al_4V rather than of Nitinol and chrome, respectively, as in the experiment. *Here, each data series measures the force felt by the tail particle rather than that of a separate load cell placed at the tapered end*. Thus, the forces felt by the last grain in this energy conserved system (basically a "worst case scenario" as alluded to earlier) are quite different than in the experiments. However, given that Nitinol is a highly energy absorptive material and that restitutive losses have been ignored, the differences in the details of Figs. 11 and 12 are understandable. By adding particles to a STC, one acquires incremental amounts of shock mitigation performance. Instead one can take that added length and split it into several particles of smaller size and interstitially disperse them such as in the DTC to see dramatic improvements in impulse dispersion.

VII. CONCLUSIONS

Granular alignments are scalable, nonlinear dynamical systems that can be constructed for highly effective shock dispersion and transmission. Their properties can be tuned by modifying the material properties and contact geometries, material mismatch, and by varying the number of grains in the alignment producing a very large number of (and sometimes unexpected) outcomes. Both the STC and the DTC systems can be experimentally realized and have been probed in some detail as reported here. We summarize below the highlights of this paper.

We have discussed here the derivation of a formula [Eq. (27)] that captures the ratio of the kinetic energy of the last grain at the tapered end to the kinetic energy of the largest grain where the impulse was incident and gives a normalized

measure of energy dispersed in the energy conserved description of the DTC. The formula has been derived in the hard-sphere approximation. It turns out that this formula fails to correctly describe the energy dispersion in the DTC by grossly overestimating energy dispersion as f, q_d, and N are increased. Interestingly, such is not the case for the corresponding formula for the STC discussed in earlier work,[8] where the formula furnishes a more reliable description of energy dispersion. A hard-sphere approximation for the STC correctly describes the functionality of N and q_s for the normalized energy parameter space. The softness of the potential is a factor but not a dominant one. The DTC, much to our surprise however, cannot be described by such an approximation because shock transmission properties vary with position along the chain and with the softness of the spheres. This particular system, consequently, cannot be treated by an independent collision model.[46] The fact that softness of the potential plays such a strong role in these size mismatched systems is, in retrospective, not a surprise and suggests that size mismatched granular chains can exhibit strongly nonlinear properties that may turn out to be quite different than in the size mismatched harmonic systems.

As a note of academic interest and in considering hard spheres, the limit of $q_d=0$ for the DTC surprisingly reduces to that for the STC under the exchange, $f \Leftrightarrow (1-q_s)$. This says that a hard-sphere chain consisting of an alternating series of radii [where $r_{small}=fr_{large}$—see Figs. 2(b), 2(d), and 2(f), for example] has the kinetic energy absorption equivalency of a STC of tapering q_s [see Fig. 1(a), for example]. A result which signifies that the shock dispersion capabilities of the STC can be easily surpassed by a chain with alternating grain sizes, not even a real DTC. For hard materials, this approximate result may be of value.

We have discussed the energetics of TCs and found that STCs (Fig. 1, top) can be loosely categorized into three groups: SW systems, shock absorption systems, and strongly oscillating systems. It has already been reported that while long, monodisperse chains support SWs, TCs act as shock absorbers. It was surprising that for small chains with some tapering, quasiperiodic and, possibly, nonlinear modal behavior seems to occur.

Our extensive dynamical simulations on impulse propagation in the DTC has been discussed in this work. A key result is that unlike harmonic systems where the light masses act as the dominant energy traps,[50] here the larger masses in the TCs (and not the interstitial grains) carry the dominant share of the energy. Thus, the interstitial particles act as the equivalent of frictional dampers as in the Brownian motion problems associated with the Langévin equation,[56] with each large mass in the DTC acting as a Brownian particle with the interstitials acting as baths. We envisage that increasing the number of interstitials could lead to better energy trapping in the larger grains. Preliminary experiments reported herein confirm that the DTC is a more efficient shock absorption system than the STC and the experimental findings are qualitatively consistent with the simulations even though the two systems are different. Experimental systems are dissipative and have chrome tapered grains and Nitinol interstitials, whereas the simulation systems are energy conserved and

have all Ti_6Al_4V grains. Further, the experimental system is open at the end where the impact is initiated, whereas the simulation system is confined within walls and that the pressure felt at the wall cannot be measured in the simulation system where a wall is not explicitly modeled.

In closing, we envision that encased STCs and DTCs can be embedded at appropriate spacings onto certain solid matrices with the system as a whole acting as a shock absorbing layer. Such layers can find applications on armored vests to protect combat personnel, combat vehicles, in protecting buildings from blasts and explosions, and perhaps even inside Wipple or bumper shields to protect spacecraft against ballistic shock issues arising from hypervelocity impacts of small-sized cosmic debris. These chains may also be adapted for use in a stacked vertical configuration to reduce the effects of impact during movement on wheel chairs when transporting injured patients.

[1] S. Abrate, *Impact on Composite Structures* (Cambridge University Press, Cambridge, 1998); M. Y. H. Bangash, *Impact and Explosion* (CRC, Boca Raton, FL, 1993); D. C. Lagoudas, K. Ravi-Chander, K. Sarh, and P. Popov, Mech. Mater. **35**, 689 (2003); Y. M. Gupta and S. Sharma, Science **277**, 909 (1997).
[2] See, for example, J. E. Bobrow, F. Jabbari, and K. Thai, J. Dyn. Syst., Meas., Control **122**, 570 (2000); E. L. Afraimovich, N. P. Perevalova, A. V. Plotnikov, and A. M. Uralov, Ann. Geophys. **19**, 395 (2001).
[3] For a general overview of surface issues for space vehicles, see J. J. DeMange, P. H. Dunlap, Jr., and B. M. Steinetz, "Advanced control surface seal development for future space vehicles," NASA Tech. Memor. Report No. 2004-212898, 2004.
[4] See, for example, in A. R. Rao, G. A. Engh, M. B. Collier, and S. Lounici, J. Bone Jt. Surg., Am. Vol. **84**, 1849 (2002).
[5] S. Sen and M. Manciu, Physica A **299**, 551 (2001).
[6] M. Nakagawa, J. H. Agui, D. Wu, and D. V. Extramiana, Granular Matter **4**, 167 (2003).
[7] A. Sokolow, J. M. M. Pfannes, R. Doney, M. Nakagawa, J. H. Agui, and S. Sen, Appl. Phys. Lett. **87**, 254104 (2005).
[8] R. Doney and S. Sen, Phys. Rev. E **72**, 041304 (2005).
[9] R. Doney and S. Sen, in *Proceedings of the 22nd International Symposium on Ballistics*, edited by W. Flis and B. Scott (DESTech, Lancaster, 2005), Vol. 9, p. 702; R. Doney, Ph.D. thesis, SUNY-Buffalo, 2007.
[10] F. Melo, S. Job, F. Santibanez, and F. Tapia, Phys. Rev. E **73**, 041305 (2006).
[11] A preliminary report on the properties of the DTC appears in R. Doney and S. Sen, Phys. Rev. Lett. **97**, 155502 (2006).
[12] T. J. Kang and C. Kim, Fibers Polym. **1**, 45 (2000).
[13] T. Niezgoda and W. Barnat, Mater. Sci. Eng., A **483–484**, 705 (2008).
[14] R. Doney and S. Sen, "Ordered granular media for shock mitigation," Army Research Laboratory Technical Report No. 3612, 2005.
[15] S. Sen, A. Sokolow, R. P. Simion, D. Sun, R. L. Doney, M. Nakagawa, J. H. Agui, Jr., and K. Shenai, *Advances in Energy Research 2007* (Macmillan, Delhi, 2007), p. 329.
[16] A. Sokolow, E. G. Bittle, and S. Sen, Europhys. Lett. **77**, 24002 (2007).
[17] R. Summers, J. Peery, M. Wong, E. Hertel, T. Trucano, and L. Chhabildas, Int. J. Impact Eng. **20**, 779 (1997).
[18] E. B. Herbold and V. F. Nesterenko, Appl. Phys. Lett. **90**, 261902 (2007).
[19] D. Gugan, Am. J. Phys. **68**, 920 (2000) (and references therein).
[20] H. Hertz, J. Reine Angew. Math. **92**, 156 (1881).
[21] K. Johnson, *Contact Mechanics* (Cambridge University Press, Cambridge, 1985).

[22]V. F. Nesterenko, J. Appl. Mech. Tech. Phys. **24**, 733 (1983); A.N. Lazaridi and V.F. Nesterenko, *ibid.* **26**, 405 (1985); V. F. Nesterenko, J. Phys. IV **C4**, 729 (1994); V.F. Neterenko, A.N. Lazaridi and E.B. Sibiryakov, *ibid.* **36**, 166 (1995).

[23]G. Friesecke and J. A. D. Wattis, Commun. Math. Phys. **161**, 391 (1994).

[24]R. S. Sinkovits and S. Sen, Phys. Rev. Lett. **74**, 2686 (1995); S. Sen and R. S. Sinkovits, Phys. Rev. E **54**, 6857 (1996); S. Sen, M. Manciu, and J. D. Wright, *ibid.* **57**, 2386 (1998).

[25]C. Coste, E. Falcon, and S. Fauve, Phys. Rev. E **56**, 6104 (1997).

[26]A. Chatterjee, Phys. Rev. E **59**, 5912 (1999).

[27]E.J. Hinch and S. Saint-Jean, Proc. R. Soc. London, Ser. A **455**, 3201 (1999).

[28]S. Sen and M. Manciu, Physica A **268**, 644 (1999); Phys. Rev. E **64**, 056605 (2001).

[29]R. M. MacKay, Phys. Lett. A **251**, 191 (1999).

[30]J. Y. Ji and J. Hong, Phys. Lett. A **260**, 60 (1999).

[31]V. F. Nesterenko, *Dynamics of Heterogeneous Materials* (Springer, New York, 2001), Chap. 1.

[32]J. Hong, Phys. Rev. Lett. **94**, 108001 (2005).

[33]C. Daraio, V. F. Nesterenko, E. Herbold, and S. Jin, Phys. Rev. Lett. **96**, 058002 (2006).

[34]F. Fraternali, M. A. Porter, and C. Daraio, "Optimal design of composite granular protectors," Mech. Adv. Mater. Structures (in press).

[35]R. Carretero-Gonzalez, D. Khatri, M. A. Porter, P. G. Kevrekidis, and C. Daraio, Phys. Rev. Lett. **102**, 024102 (2009).

[36]It is fairly inexpensive to bulk purchase chrome ball bearings. D. DiCocco and S. Sen, DTC apparatus, SUNY Buffalo. The cost associated with materials was approximately USD 50.

[37]R. Frey, private communication (2005).

[38]B. A. Gama, T. A. Bogetti, B. K. Fink, C. J. Yu, T. D. Claar, H. H. Eifert, and J. W. Gillespie, Jr., Compos. Struct. **52**, 381 (2001).

[39]A. Hayes, A. Wang, B. Dempsey, and D. McDowell, Mech. Mater. **36**, 691 (2004).

[40]H. Bruck, Int. J. Solids Struct. **37**, 6383 (2000).

[41]S. Sen, J. Hong, J. Bang, E. Avalos, and R. Doney, Phys. Rep. **462**, 21 (2008).

[42]The virial theorem, as presented for instance in H. Goldstein, C. Poole, and J. L. Safko, *Classical Mechanics*, 3rd ed. (Addison-Wesley, San Francisco, 2002), immediately allows one to write a conservative system's kinetic and potential energy in terms of its total energy; thus, virial theorem demands that for potentials of the form $V(\delta) \propto \delta^n$, one can write the average kinetic energy $\langle K \rangle = [n/(n+2)]E$, and the average potential energy as $\langle V \rangle = [2/(n+2)]E$, where E is the total energy. For $n=5/2$, $\langle K \rangle = \frac{5}{9}E$ which is $\approx 55.5\%$ of total energy.

[43]References 22, 31, and 41 present detailed analyses to show that the Hertz potential between grains in a system without precompression is nonperturbative in nature. This means that one cannot carry out a Taylor expansion of this potential and pull out a leading order harmonic term for "small compressions" of the grains. Thus, any perturbation produces nonlinear waves in these systems (again discussed in Refs. 22, 31, and 41). For small chains, we believe that these nonlinear effects alter the ability of the system to get compressed and hence departure from hard-sphere approximation studies become significant.

[44]The alloy material Ti_6Al_4V is known for being light and strong, especially with increasing temperatures; see, for example, L. Qian, X. Xiao, Q. Sun, and T. Yu, Appl. Phys. Lett. **84**, 1076 (2004); **86**, 129901(E) (2005); we assume that an impact at 10 m/s does not significantly deform the grains so as to drive them into the plastic regime in such a material. However, even if this velocity were to be inappropriately large for our grains in experiments, the results presented here, except those in Figs. 11 and 12, which are all normalized, would be valid for comparison with data in the elastic regime.

[45]M. P. Allen and D. J. Tildesley, *Computer Simulation of Liquids* (Clarendon, Oxford, 1987).

[46]D. T. Wu, Physica A **315**, 194 (2002).

[47]S. Wolfram, Phys. Rev. Lett. **55**, 449 (1985).

[48]M. Tabor, *Chaos and Integrability in Nonlinear Dynamics: An Introduction* (Wiley-Interscience, New York, 1989).

[49]See, for example, R. M. Rosenberg, Adv. Appl. Mech. **9**, 155 (1966); *Normal Modes and Localization in Nonlinear Systems*, edited by A. F. Vakakis (Kluwer, Dordrecht, 2001).

[50]M. H. Lee, J. Florencio, and J. Hong, J. Phys. A **22**, L331 (1989).

[51]S. Job, F. Melo, A. Sokolow, and S. Sen, Granular Matter **10**, 13 (2007).

[52]M. Manciu, S. Sen and A.J. Hurd, Physica A **274**, 588 (1999); **274**, 607 (1999).

[53]The Nitinol spheres were made available to us by J. Jullen, Nitinol Technologies, Inc.

[54]S. Job, F. Melo, A. Sokolow, and S. Sen, Phys. Rev. Lett. **94**, 178002 (2005).

[55]A. Rosas, A. H. Romero, V. F. Nesterenko, and K. Lindenberg, Phys. Rev. Lett. **98**, 164301 (2007).

[56]S. Sen, Physica A **360**, 304 (2006).

NO. OF
COPIES   ORGANIZATION

  1   DEFENSE TECHNICAL
 (PDF   INFORMATION CTR
 only)   DTIC OCA
         8725 JOHN J KINGMAN RD
         STE 0944
         FORT BELVOIR VA 22060-6218

  1   DIRECTOR
         US ARMY RESEARCH LAB
         IMNE ALC HRR
         2800 POWDER MILL RD
         ADELPHI MD 20783-1197

  1   DIRECTOR
         US ARMY RESEARCH LAB
         RDRL CIM L
         2800 POWDER MILL RD
         ADELPHI MD 20783-1197

  1   DIRECTOR
         US ARMY RESEARCH LAB
         RDRL CIM P
         2800 POWDER MILL RD
         ADELPHI MD 20783-1197

         ABERDEEN PROVING GROUND

  1   DIR USARL
         RDRL CIM G (BLDG 4600)

NO. OF
COPIES ORGANIZATION

    1   US ARMY RSRCH OFC
          B LAMATTINA
          RESEARCH TRIANGLE PARK NC
          27709-2211

          ABERDEEN PROVING GROUND

    5   DIR USARL
          RDRL WMP
            P BAKER
          RDRL WMP A
            C HUMMER
            J POWELL
          RDRL WMP D
            G VUNNI
          RDRL WMP E
            C KRAUTHAUSER